[American Journal of Science, Vol. 312, February, 2012, P. 90–116, DOI 10.2475/02.2012.02]

TOPOGRAPHIC EVOLUTION OF THE SIERRA NEVADA MEASURED DIRECTLY BY INVERSION OF LOW-TEMPERATURE THERMOCHRONOLOGY

DEVIN MCPHILLIPS* and MARK T. BRANDON**

ABSTRACT. At present, there are at least two competing ideas for the topographic evolution of the Sierra Nevada. One idea is that the Sierra Nevada was formed as a monocline in the Cretaceous, marking the transition from the Great Valley forearc basin to the west, and a high Nevadaplano plateau to the east, similar to the west flank of the modern Altiplano of the Andes. Both the thermochronologic imprint of local relief and the stable isotopic evidence of a topographic rain shadow support this hypothesis. A second idea, supported by geomorphic observations, suggests that the Sierra gained a large fraction of its present elevation as recently as the Pliocene. This recent surface uplift could have been driven by convective removal of the lower part of the lithosphere, the isostatic response to Basin and Range faulting, and/or by changes in dynamic topography associated with deep subduction of the Farallon plate. Here we present the first comprehensive analysis of low-temperature thermochronology in the Sierra Nevada, which indicates that both ideas are likely correct. We show that thermochronology can resolve surface uplift as well as exhumation by measuring long-wavelength topographic evolution relative to sea level. Uplift measurements are possible whenever there is sufficient constraint on vertical rock velocity. The tilting of isochrones, defined as surfaces of equal cooling age, provide this constraint in the Sierra Nevada. Three new factors further distinguish our analysis. The first is that we allow for the local relief and the long-wavelength topography to evolve independently. Second, we use Al-in-Hb barometry to constrain the initial depth of emplacement for the Sierra Nevada plutons. Third, our analysis is tied to a sea-level datum by using the paleo-bathymetric record of the Great Valley basin, where it transitions to the Sierra Nevada batholith. Results indicate that westward tilting of the Sierra Nevada accounts for 2 km of uplift since 20 Ma. Topographic relief increased by a factor of 2. These findings suggest that the Sierra Nevada lost elevation through most of the Tertiary but regained much of its initial elevation following the onset of surface uplift in the Miocene.

Key words: thermochronology, paleoelevation, Sierra Nevada, isochrone

INTRODUCTION

The western United States has as much as 9 km of vertical relief from the offshore abyssal plain to the peaks of the Cordillera (fig. 1). Nearly half of the elevation gain is achieved over about 150 km between the eastern Great Valley and the crest of the Sierra Nevada. The evolution of this dramatic topography remains controversial. One interpretation favors high-elevation Cretaceous topography that slowly decayed throughout the Cenozoic to its present, relatively low-elevation state (House and others, 1998; Poage and Chamberlain, 2002; Stock and others, 2005; Mulch and others, 2006; Mulch and others, 2008; Cassel and others, 2009; Hren and others, 2010; Cassel and others, 2012). The alternative calls for elevation gains of 1 to 2 km in the late Cenozoic, implying much lower elevations in the Eocence and Oligocene (LeConte, 1886; Huber, 1981; Unruh, 1991; Wakabayashi and Sawyer, 2001; Clark and others, 2005). The controversy persists because of the difficulties of measuring paleoelevation. For example, stable isotope proxies are susceptible to biases due to diagenesis and climate change (Mulch and

* Department of Geology, University of Vermont, Burlington, Vermont 05405; devin.mcphillips@gmail.com
** Department of Geology and Geophysics, Yale University, New Haven, Connecticut 06520-8109

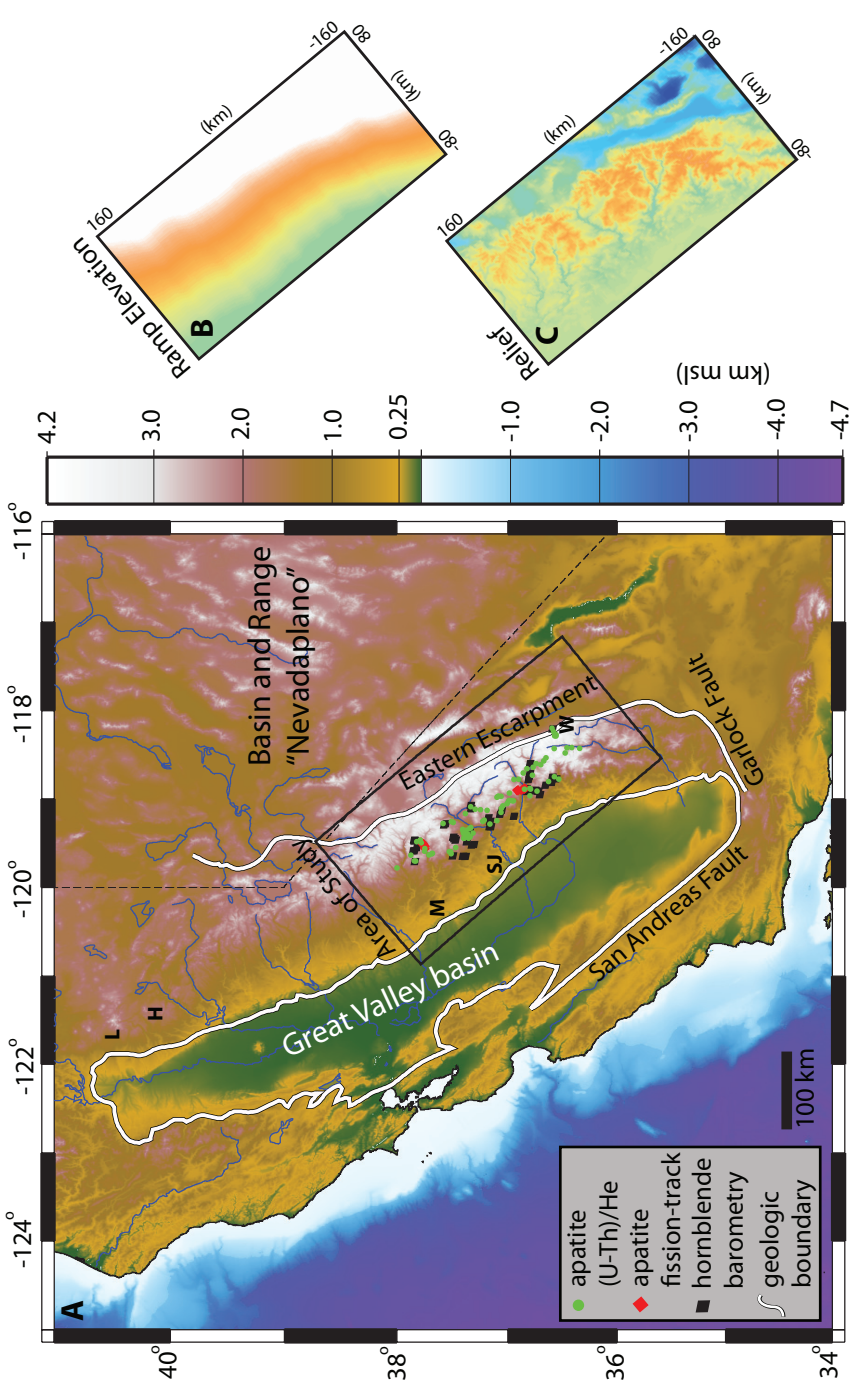

Fig. 1. The topography of the western United States. (A) The study area is outlined in black and all of the 149 measurements used in the inverse are shown (Dumitru, 1990; House and others, 1997, 1998, 2002; Ague and Brimhall, 1988). The westward tilt of the Sierra Nevada topographic surface is also visible. In the eastern Great Valley, the lithologic transition from sedimentary deposits to Mesozoic plutons closely follows the topography at a contour of ~200 m. (B) The mean topographic surface within the study area. (C) Relief around mean surface. The modeling treats these components of topography independently.

Chamberlain, 2007; Molnar, 2010). Geologic and geomorphic evidence do provide convincing evidence of local tilting and incision, but these observations are hard to link to topographic evolution at the regional scale. Here, we contribute a new measurement of paleoelevation, derived directly from low-temperature thermochronology.

The present controversy is partly a debate over the origin of high topography generally, which is increasingly recognized as the result of more than just crustal thickening associated with plate convergence. Convective forces in the mantle can support large dynamic topography at the surface (Mitrovica and others, 1989; Liu and Gurnis, 2010). In the Sierra Nevada, these forces could plausibly account for 1 to 2 km of the present elevation (Lowry and others, 2000). The removal of the lower lithosphere is capable of similar contributions to the elevation of mountain belts (Houseman and others, 1981; Göğüs and Pysklywec, 2008). The Sierra Nevada is one of the few locations with concrete evidence for lithosphere drips at the scale large enough to drive significant topographic elevation gains (Ducea and Saleeby, 1996; Jones and others, 2004; Zandt and others, 2004; Le Pourhiet and others, 2006). An isostatic response to extension and faulting has also been proposed as a source of elevation in the Sierra Nevada (Chase and Wallace, 1986; Thompson and Parsons, 2009). However, reliable estimates of paleoelevation are required to test these predictions. Large surface uplift in the late Cenozoic, after the cessation of subduction, would require a driver other than horizontal convergence and crustal thickening.

The objective of this paper is to unravel the topographic evolution of the Sierra Nevada using low-temperature thermochronology. The prevailing view is that thermochronology can only measure erosion, not surface uplift (for example, England and Molnar, 1990; Reiners, 2007). We show here that, in some cases, thermochronology can be used to estimate the evolution of paleotopography at a regional scale. We begin by reviewing the controversy surrounding surface uplift in the Sierra Nevada. Next, we discuss the results from our previous study, which show that isochrones, or surfaces of equal cooling age, tilt uniformly to the southwest (McPhillips and Brandon, 2010). The isochrone concept is particularly important for the analysis presented here because the tilting is a measure of rock uplift. The data require a unique surface elevation history because they constrain both exhumation and rock uplift. The eastern boundary of the Great Valley provides a stable sea-level datum for this measurement. We then introduce the coupled thermal-kinematic model Pecube (Braun, 2003), along with several important changes to its standard parameterization, in order to provide a full analysis of the data. The Neighborhood Algorithm (NA) (Sambridge, 1999a; Sambridge, 1999b) provides a comprehensive exploration of the parameter space as well as best estimates and uncertainties for the model parameters. Our results show a two-stage topographic history for the southern Sierra Nevada, starting with an Andean-scale topography at ~100 Ma, followed by a slow two- to three-fold reduction in topography, and then a growth of new topography starting at about 20 Ma. Since then, peak elevations have increased by 2 km, producing the present topography of the region.

BACKGROUND

The Sierra Nevada is a large batholith, which has been exposed by differential exhumation in its southern half (Ague and Brimhall, 1988). In the north, exposures of stratigraphically overlying Tertiary volcanics and non-marine sediments are frequently preserved. The batholith was formed in association with Mesozoic subduction along the western margin of North America (Evernden and Kistler, 1970; Stern and others, 1981; Chen and Moore, 1982). This tectonic setting suggests some form of high topography in the Cretaceous. The plutonism occurred between 110 to 90 Ma. Subsequently, the Sierra Nevada arc became inactive, perhaps due to shallow subduction by the Farallon plate (Dickinson and Snyder, 1979) and/or the northward migration of the Baja BC block, which was bounded on its west side by a subduction

zone (Cowan and others, 1997; Miller and others, 2006). As a result, the thermal evolution of the shallow crust was mainly controlled by cooling during exhumation. The San Andreas transform boundary started to grow at about 35 Ma, and has gradually replaced much of the older subduction boundary along the western side of California and Mexico (Atwater and Stock, 1988). Normal faulting associated with Basin and Range extension arrived in the Pliocene with the formation of Owens Valley and the Eastern Sierra Escarpment (Bachman, 1978).

The sedimentary strata of the Great Valley record its elevation since the Cretaceous. Large areas of what is now the Great Valley were deposited at bathyal depths of several kilometers or on a steep, narrow continental slope (Ingersoll, 1979; Cherven, 1983; Mitchell and others, 2010). However, shallow marine, estuarine, and beach deposits indicate that the eastern margin of the Great Valley has persisted near sea level since at least 85 Ma (Ingersoll, 1979; Bartow, 1991). Transgressions of at most a few hundred meters occurred locally (Oslon, 1988). In effect, the boundary between the Great Valley and the southern Sierra Nevada provides a stable, sea-level reference frame for nearly the entire evolution of the Sierra Nevada.

The present topography of the Sierra Nevada has the profile of a tilted block, where a wide, shallow western slope contrasts with the steep Eastern Sierra Escarpment (fig. 1). To the west of this fault zone, the Sierra Nevada batholith is essentially unbroken by faults or other structural features (Dixon and others, 2000). A southward trend toward higher elevation is superimposed on the overall east-side-up tilt of the range. Modern peak elevations show a steady progression from 2.1 km at Humboldt Peak in the north to 4.4 km at Mt. Whitney in the south. Likewise, relief at the scale of drainage basins increases from <1 km to >2 km over the same distance. These north-south differences have led some to propose somewhat different elevation histories for the north and south (Wakabayashi and Sawyer, 2001; Mulch and others, 2008). Our analysis focuses on the southern Sierra Nevada, often called the High Sierra, spanning from the Merced River in the north to Mt. Whitney in the south (fig. 1). We exclude the southernmost Sierra, which has an independent history associated with the Garlock and San Andreas faults (Maheo and others, 2009).

Early research constrained the age of tilting to the late Cenozoic and suggested that tilting created much of the present topography (LeConte, 1886; Lingren, 1911). Subsequent research has reinforced these results (Huber, 1981; Unruh, 1991; Wakabayashi and Sawyer, 2001). The main argument is that the dip of Cenozoic features in the northern Sierra Nevada, including both the easternmost Great Valley sedimentary strata and the preserved remnants of stream channels in the batholith, reflect the block-tilting around a hinge in the eastern Great Valley at ~10 to 5 Ma (Huber, 1981; Unruh, 1991; Wakabayashi and Sawyer, 2001). The relevant strata and surfaces are only preserved to the north of the San Joaquin River. Evidence from throughout the Sierra shows a pulse of stream incision at this time, consistent with an increase in gradient (Wakabayashi and Sawyer, 2001; Stock and others, 2004; Stock and others, 2005; Clark and others, 2005). Although none of this evidence is sufficient to constrain the absolute paleoelevation of the Sierra crest, it suggests as much as 2 km of peak surface uplift since ~10 Ma. Stock and others (2004, 2005) argue that most of the relief in southern river canyons predates Pliocene incision, indicating that substantial early topography was also present.

Coney and Harms (1984) hypothesize that high Cretaceous topography collapsed in the Tertiary in order to explain the formation and prevalence of metamorphic core complexes in the western U.S. Seismic surveys showing anomalously thin crust under the southern Sierra Nevada and adjacent Basin and Range support Tertiary thinning (Wernicke and others, 1996). In an early application of thermochronology to topography, House and others (1998) interpret transects of apatite cooling ages to suggest that

the Late Cretaceous mean topographic elevation of the southern Sierra Nevada was nearly twice as high as the present. The apatite closure isochrone appears to have been distorted within the southern batholith by about 70 Ma (House and others, 1997; House and others, 1998; House and others, 2001). House and others (1998) interpret this distortion as the result of large canyons aligned with the modern San Joaquin and Kings Rivers and extrapolate paleoelevation from their relief. Together, these results suggest that the Sierra Nevada was a monocline in Cretaceous time, which ramped up from sea level at the boundary of the Great Valley to a high interior plateau. This plateau is sometimes referred to as the Nevadaplano by analogy to the modern Andean Altiplano (DeCelles, 2004). Recent studies of sediment provenance try to pinpoint the location of the headwaters of Eocene rivers (Cecil and others, 2010; Cassel and others, 2012). Cassel and others (2012) argue convincingly that Eocene alluvial deposits in California were sourced by large fluvial systems that originated far to the east of the modern Sierra crest, perhaps on the former Nevadaplano plateau.

The recent application of stable isotope proxies presents a somewhat similar picture. In the northern Sierra, these proxies show evidence of high topography since at least Eocene time (Poage and Chamberlain, 2002; Mulch and others, 2006; Mulch and others, 2008; Cassel and others, 2009; Hren and others, 2010). Relatively sparse data in the south support high topography since at least the middle Miocene (Crowley and others, 2008; Mulch and others, 2008). Recent compilations of stable isotope data from throughout the western Cordillera have been interpreted as showing the diachronous growth of high topography through the Eocene and Oligocene (Mix and others, 2011; Chamberlain and others, 2012). All of these proxies infer paleoelevation from systematic isotope fractionation between low and high topography. Although all stable isotope proxies are subject to biases related to changing climate conditions (Mulch and Chamberlain, 2007; Molnar, 2010; Poulsen and Jeffery, 2011), the analyses of ancient clay, volcanic glass, and organic molecules yield similar results.

Among mechanisms proposed for recent uplift, asthenosphere buoyancy (that is, dynamic topography), the removal of dense lithosphere, and the isostatic response to faulting are perhaps the most credible. Different estimates of dynamic topography (which are not always exclusive) yield a wide range of contributions, from 0.1 to 2 km to the present surface elevation (Mitrovica and others, 1989; Lowry and others, 2000; Moucha and others, 2009; Liu and Gurnis, 2010). In the southern Sierra, volcanic xenoliths show a change in mantle composition from pyroxenite to peridotite sometime between 8 and 3 Ma (Ducea and Saleeby, 1996; Lee and others, 2001), and seismic imaging appears to capture a dense body sinking into the mantle, called the Isabella Anomaly (Ruppert and others, 1998; Zandt and others, 2004). Jones and others (2004) show that the removal of dense lower lithosphere could account for nearly all of the inferred late Cenozoic surface uplift. Although there appears to be a seismic velocity anomaly in the north similar to the Isabella Anomaly (Benz and Zandt, 1993), receiver functions only resolve a drip through the Moho in the south (Frassetto and others, 2010). The northern Sierra also lacks petrologic evidence for a drip (Jones and others, 2004), implying that unstable lithosphere might be restricted to the south. Finally, the response of the crust to Basin and Range extension and faulting has been proposed as a source of uplift. Although the elastic thickness of the crust is probably too small to satisfy the flexural model of Chase and Wallace (1986), Thompson and Parsons (2009) show that isostatic support could provide more than 1 km of uplift following the onset of faulting on the Eastern Sierra Escarpment.

CONSTRAINTS ON SURFACE UPLIFT FROM THERMOCHRONOLOGY

Isochrone Conceptual Model

In order to use low-temperature thermochronology to measure surface uplift, we rely on isochrones, or surfaces of equal cooling age. This idea goes back to the early

thermochronologic studies [for example, Armstrong (1982) used the term "chrontours" to describe the pattern of cooling ages around metamorphic core complexes]. We use the term isochrones to emphasize that a cooling age is a point-wise sample of a specific cooling age surface. These surfaces are formed as rocks cool while moving through a thermal window, called the partial retention zone (PRZ). This window spans a temperature interval of about 10 to 30 °C for most low-temperature thermochronometers (Reiners and Brandon, 2006). The isochrone surface is fully formed only after it cools through this window. Dodson (1973) showed that for the case of monotonic cooling, cooling age may be related to an effective closure temperature, which is a function mainly of the diffusion properties of the radiogenic production in the mineral host, and the rate of cooling in the PRZ. Non-monotonic cooling histories are commonly observed in sedimentary basins, but erosion in upland landscapes tends to result in monotonic cooling through the PRZ. As a result, we can use the Dodson concept to define an effective closure isochrone, which would be the initial "zero-age" surface where an isochrone was formed.

For a given thermochronometer with uniform closure properties, we would expect the closure isochrone to follow a specific isothermal surface. Although the closure isochrone can rise or fall relative to the isothermal surfaces due to spatial and temporal variations in cooling rates, thermal-kinematic modeling indicates that the closure isochrone should usually have low relief, generally much smaller than the relief of the overlying topography. Thus, we can envision these surfaces by analogy to sedimentary bedding. Sedimentary beds also form as nearly flat planes with the minimum gradients necessary to transport sediment (for example, the depositional gradient; Leopold and Bull, 1979). As rock is exhumed, isochrones are continuously created and advected toward the surface, thereby populating the crust. The isochrone conceptual model is frequently used implicitly in thermochronology, for example when interpreting age-elevation relationships (Wagner and Reime, 1977; see also McPhillips and Brandon, 2010). By treating isochrones explicitly, we are able to measure rock uplift as well as exhumation, thereby constraining surface uplift and paleoelevation.

End-Member Cases

In order to measure the uplift of a topographic surface, England and Molnar (1990) argue that it is necessary to know both rock uplift and exhumation rates. The rate of rock uplift is defined as the vertical component of the velocity of a particle of rock, measured with respect to the initial position of the particle. In contrast, exhumation rate is defined as the vertical component of rock velocity, measured with respect to the topographic surface. As England and Molnar (1990) point out, individual thermochronologic ages only measure exhumation rate. (Note that erosion is commonly the dominant exhumation process in the shallow crust of convergent orogens.) However, in the Sierra Nevada, McPhillips and Brandon (2010) show that the suite of apatite (U-Th)/He data define isochrones that are well approximated by a tilted stack of parallel planes. These planes are oriented subparallel to the present topographic surface, but with a steeper dip (3.4° versus 1.8°). The observation of dipping isochrones provides a prior constraint on rock uplift rates as well as erosion rates. We illustrate this constraint by considering two different ways to form tilted isochrones. From these simple end-members, we then develop a model parameterization to evaluate the topographic evolution of the Sierra Nevada.

In the first end-member, erosion maintains steady state topography identical to the modern form. As a result, isochrones form parallel to a relatively flat closure isotherm (as estimated by Pecube), and deformation is required to produce tilting steeper than topography (fig. 2A). Either rigid rotation or vertical shear could tilt isochrones. The observed isochrone dip records total rock uplift, and the individual

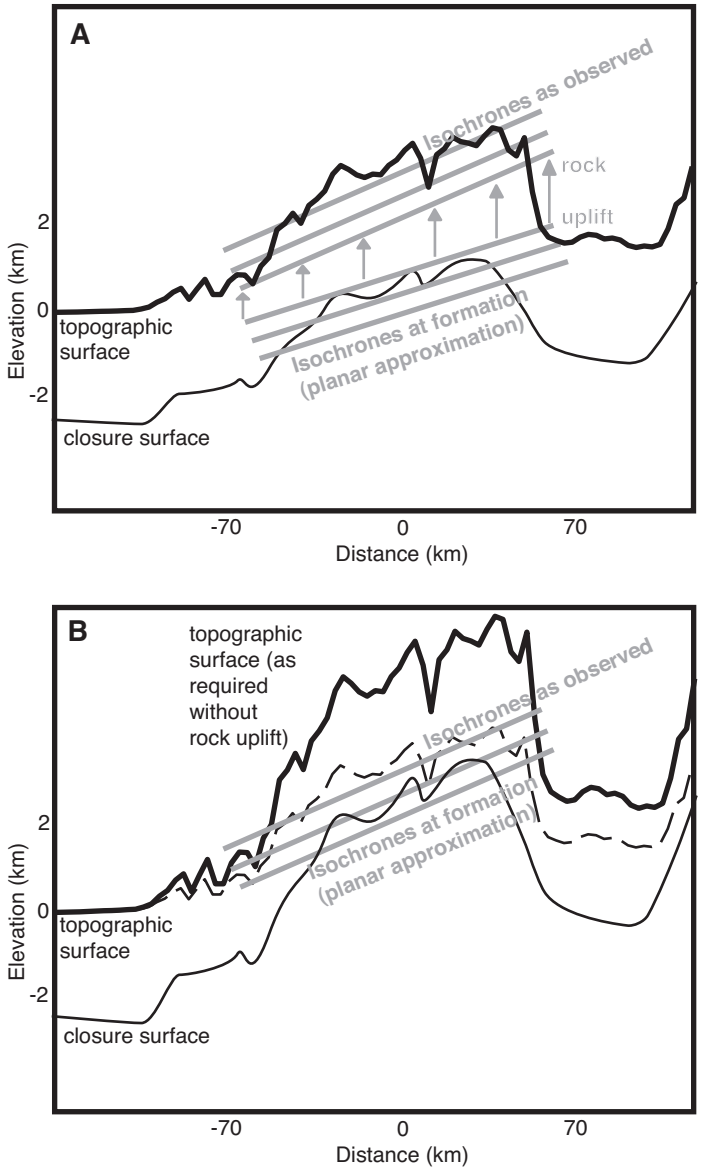

Fig. 2. Schematic illustration of the end-member formations of dipping isochrones. Isochrones are surfaces of equal cooling age in the crust. Two end-members cases illustrate the range of processes for creating planar, tilted isochrones. (A) Strain associated with a gradient in rock uplift rates may cause isochrones to dip after their formation at the closure isotherm. (B) Topography may create a dip, as it warps the closure isotherm and subsequently erodes away.

cooling ages record local exhumation. Surface uplift is constrained jointly by these two components.

In the second end-member, the rock uplift rate is zero and topography is not isostatically compensated. As a large mountain range decays, erosion gradually exhumes isochrones from depth. Eventually, the exposed isochrones dip more steeply than surrounding topography (fig. 2B). This is because shallow isotherms, potentially

TABLE 1
Fixed model parameters

Elastic thickness	12 km	Lowry and others, 2000 Granger and Stock, 2004
Crust density	2700 kg/m^3	Christensen and Mooney, 1995
Mantle density	3200 kg/m^3	Christensen and Mooney, 1995
Young's modulus	1.e11 Pa	Christensen and Mooney, 1995
Poisson's ratio	0.25	Christensen and Mooney, 1995
Thermal diffusivity	27.6 km^2/Myr	Lachenbruch and Sass, 1977
Heat production	8.8 °C/Myr	Brady and others, 2006
Sea level surface temperature	15.9 °C	Miller and others, 2006
Atmospheric lapse rate	3.4 °C/km	Miller and others, 2006

including the isotherm at the closure temperature, closely track the long-wavelength topographic surface (Mancktelow and Grasemann, 1997). The exposed isochrones preserve the relatively steep dip that was imposed during closure by the initially high topography (fig. 2B). The western slope of the Sierra Nevada is wide enough to impose a large fraction of its dip on the shallow thermal field, including the apatite (U-Th)/He closure isochrone. Without isostatic compensation, the observed isochrone dip would require an ancient mountain range approximately twice as high as the modern Sierra Nevada. The omission of isostasy simplifies this scenario for the purpose of illustration, but any realistic model must include isostasy.

MODELING AND INVERSION

Thermal-Kinematic Model

The model Pecube solves the 3-dimensional heat transport equation:

$$\rho c\left(\frac{\partial T}{dt} + \nu \frac{\partial T}{dz}\right) = \frac{\partial}{\partial x} k \frac{\partial T}{\partial x} + \frac{\partial}{\partial y} k \frac{\partial T}{\partial y} + \frac{\partial}{\partial z} k \frac{\partial T}{\partial z} + \rho H, \quad (1)$$

subject to an evolving topographic surface and arbitrary field of rock uplift rates (Braun, 2003). We parameterize the topographic surface and the rock uplift rates and invert to find their evolution, described in detail below. For data, we use 88 apatite (U-Th)/He ages (Dumitru, 1990; House and others, 1997, 1998, 2001; Clark and others, 2005), 15 apatite fission-track ages (Dumitru, 1990), and 46 Al-in-hornblende barometry measurements (Ague and Brimhall, 1988) from the literature, thereby constraining both low-temperature cooling and total exhumation in the batholith. Pecube calculates cooling ages at the surface directly from Lagrangian time-temperature paths. Pecube also accounts for relevant thermal and rheological parameters, which we estimate from the literature (table 1). Preliminary experiments suggest that the inverse estimates are not sensitive to these choices. Thermal conductivity deserves special attention because it is known to vary among the Sierra plutons (Brady and others, 2006). We choose a single, intermediate value. Calculations using the 1-dimensional, steady state model Age2Edot (Brandon in Ehlers and others, 2005)

show that the widest range of observed conductivities can account for no more than 30 percent of the observed isochrone dip, even when the variance in conductivity is arranged systematically down-dip.

We run Pecube on 3 km grid, which is sufficient to capture 99 percent of the variance in the depth of the apatite (U-Th)/He closure isochrone (fig. 3). While this relatively coarse grid was sufficient for the thermal problem, it filters out some local topographic relief. Pecube must be modified to account for the interpolation of ages over smoothed topographic data, especially in slowly eroding regions like the Sierra Nevada. If not, a cooling age sited on a local promontory could be modeled at an elevation of hundreds of meters lower than the observed topography. This amount of smoothing corresponds to an age difference of several million years when erosion rates are low. To address the issue, we calculate the predicted age for the observed elevation using the interpolated model topography and the vertical age gradient at each point. We find that in the case of the Sierra Nevada this correction improves the misfit by 5 to 10 percent.

There is a growing literature exploring the possible effects of radiation damage on the diffusion of helium in a crystal lattice (Farley, 2000; Shuster and others, 2006; Shuster and Farley, 2009; Flowers and others, 2009; Gautheron and others, 2009; Cherniak and others, 2009). Pecube does not account for radiation damage effects when calculating (U/Th)/He cooling ages (Braun, 2003), and we do not add a damage model to the Pecube calculations. Although the cooling ages in the Sierra Nevada are old enough to have accumulated significant radiation damage, the apatite crystals have low concentrations of parent isotopes (House and others, 1997, 1998, 2001). As a result, too few decay events have occurred for radiation damage to have played an important role in helium diffusion in the Sierra. A simple test is proposed by Flowers and others (2009): plotting eU concentration against apatite (U-Th)/He age. Flowers and others (2009) argue that significant damage effects will manifest as a positive, non-linear correlation, which is absent in the Sierra Nevada data (fig. 4).

Parameterization

The model Pecube is designed primarily to calculate exhumation rates and changes in local relief (Braun, 2003). The model requires modification in order to invert for Sierra Nevada paleotopography. As a starting point, we use the observation of tilted isochrones in the apatite (U-Th)/He system (McPhillips and Brandon, 2010). The end-member cases described above illustrate how this tilt could be produced by gradients of either rock uplift or exhumation across the strike of the Sierra Nevada. Our aim is to parameterize the simplest model capable of capturing the continuous transition between these two end-members.

Sedimentary evidence shows that the eastern boundary of the Great Valley forms a stable sea-level reference frame since at least 85 Ma (Dickinson and others, 1979; Bartow, 1991). As a result, both the rock uplift and exhumation rates along this line have been near zero for most of its history. Sedimentation rates were (Moxon and Graham, 1987) near steady state relative to the depositional surface. (A depositional rate of 100 m/Ma gives a Peclet number <0.1, so the thermal field can be approximated as purely conductive.) Therefore, the boundary may be viewed as a hinge line for the isochrone tilting, just as it is often used to approximate the hinge line for tilting estimates in the geomorphology literature (Huber, 1981; Unruh, 1991; Wakabayashi and Sawyer, 2001).

The tilted isochrones presently have the form of a topographic ramp that would reach above the modern peaks if projected from the eastern boundary of the Great Valley. The ramp is approximately parallel to the Eocene Ione Formation where it is exposed at this boundary (Unruh, 1991), although it is steeper than the slope of the

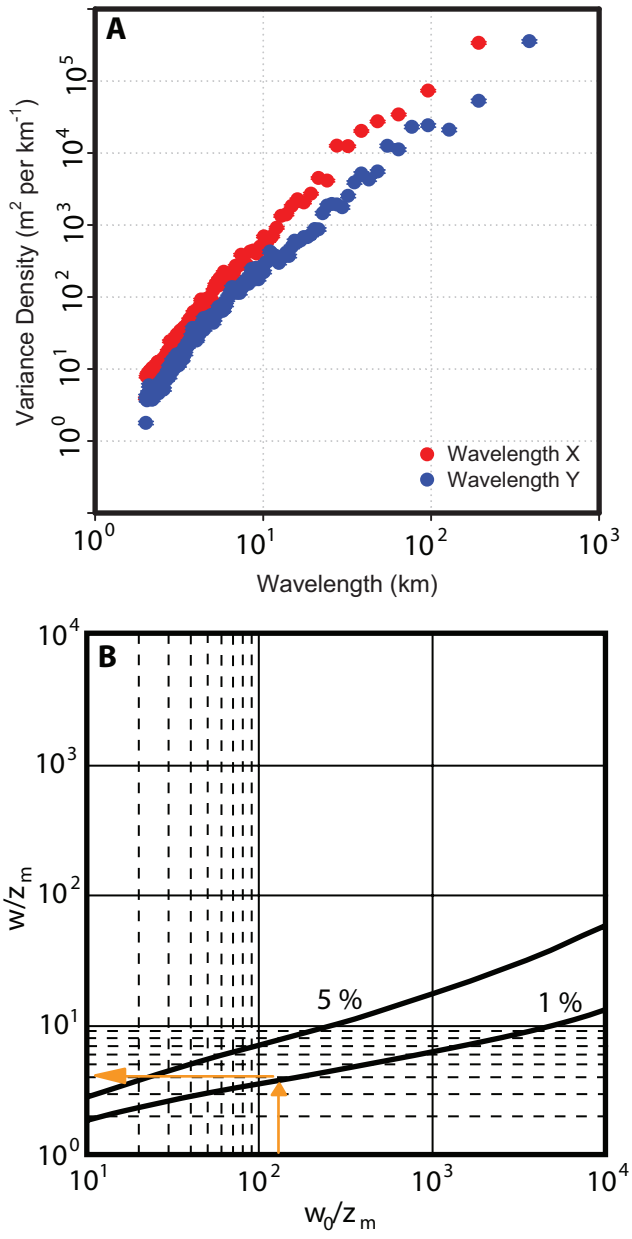

Fig. 3. (A) The variance density distribution of the Sierra Nevada as a function of wavelength. The topography shows a Brownian variance distribution (Huang and Turcotte, 1990). (B) The integrated variance for the topography of the closure surface, as integrated over the range of wavelengths, w, from the smallest to the largest wavelength, w_0, present in the digital elevation model of the Sierra Nevada (30 m resolution). The integrated variance assumes a Brownian distribution for the surface topography and the attenuation of the surface topography when downward continued to a closure depth, z_m. The arrows show that for the Sierra Nevada, which has $w_0 \sim 200$ km, the digital data should represent wavelengths down to 4 km to capture 99% of the topographic variance on the closure boundary.

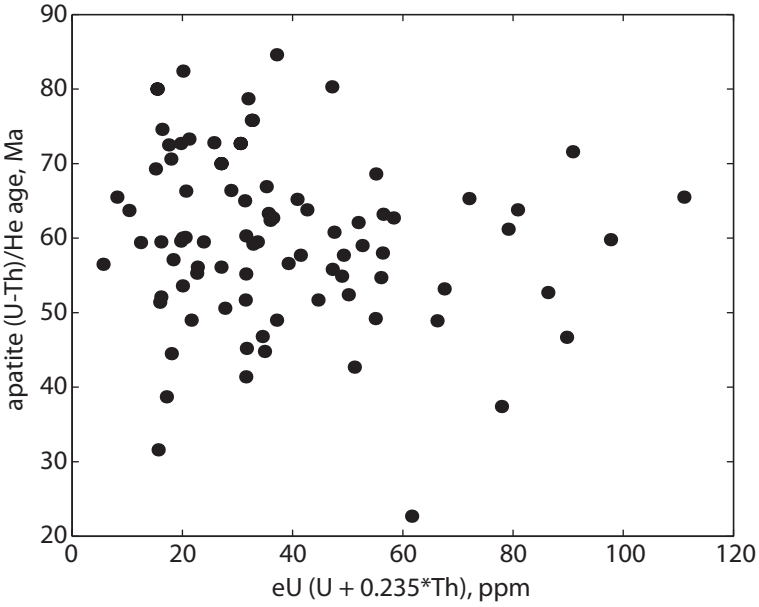

Fig. 4. Test of radiation damage effect on helium diffusion. Following Flowers and others (2009), we test for significant effects from radiation damage by plotting eU concentration against apatite (U-Th)/He age. Flowers and others (2009) argue that significant damage effects will manifest as a positive, non-linear correlation, which is absent here.

present topographic surface. As illustrated by the end-member cases, the rock uplift rate and/or the ancient topographic surface must "ramp-up" (that is, systematically increase) between the boundary of the Great Valley and the crest of the Sierra Nevada in order to produce the observed tilting. We take advantage of this fact and parameterize both rock uplift rate and topography with a ramp-like form.

Topography is decomposed into two parts. The first is the sloping mean elevation surface between the boundary of the Great Valley and the Eastern Sierra Escarpment (fig. 1B). This is the topographic ramp. The second part is the variance around the mean surface (fig. 1C). This is local relief. The actual elevation of topography is given by the sum of these two parts. Past topography is parameterized in terms of two multiplicative factors that scale the topographic ramp and local relief, respectively, relative to the modern topography: *rampElevation* and *relief* (table 2). This decomposition provides a more realistic parameterization than a single value because local relief and the tilting of the mean topography are allowed to evolve independently.

The topographic parameters define the state of topography at specific times in the past. Topography evolves linearly between these states. At minimum, one set of topographic parameters is required in order to define the initial state. The final state is always given by the modern values. Additional topographic states may be defined between the initial and final states. An additional state requires an additional free parameter for time. In our preferred model parameterization, the topographic parameters are defined for three states: initial (*time0*), intermediate (*time1*), and final (*time2*). Only *time1* is a free parameter in the inverse. We use the Bayesian Information Criterion (Schwarz, 1978; Liddle, 2008) in order to select the number of topographic states and the value of *time0* to use. Table 2 summarizes our preferred parameterization scheme.

TABLE 2
Model free parameters

Stage in model time	Topographic relief	Mean topographic surface	Tectonic rock uplift (between time stages)	Temperature at model base (at 50 km, for all time stages)
time0	*relief0*	*rampElevation0*		
			tectonicUplift0	
time1	*relief1*	*rampElevation1*		*basalTemp*
			tectonicUplift1	
time2	*relief2*	*rampElevation2*		

Rock uplift is also decomposed into two parts, flexural and tectonic. The flexural component is defined implicitly by changes in the topographic load, such that the rock uplift rate includes the value necessary to maintain compensation between topographic states. For the tectonic component of rock uplift, we rely on the idea of a ramp. Tectonic rock uplift persisted near zero at the boundary of the Great Valley, even though it may have been much higher under the crest of the Sierra Nevada. We parameterize this contrast using a ramp function that mirrors the form of the mean topographic surface (fig. 5). The parameter *tectonicUplift* scales the function according to the maximum rock uplift at the topographic crest. The form of the function ensures that rock uplift decreases monotonically toward the Great Valley, where it is zero. The value of *tectonicUplift* gives the maximum amount of vertical displacement of rock (in kilometers) between successive topographic states, not including flexure.

Inversion

For the inverse problem, we employ a direct search method to constrain parameters of interest. For efficiency, we apply the Neighborhood Algorithm, which uses nearest-neighbor calculations to concentrate sampling in the regions of the multidimensional parameter space that yield low misfit values (Sambridge, 1999a; for application to thermochronology, see Herman and others, 2010). A fraction of the samples (here, 50%) is also selected at random in order to avoid local minima. Misfit is quantified as the standard deviation of the residuals, which is defined as:

$$\sigma = \sqrt{\sum_i (\tau_i^{obs} - \tau_i^{pred})^2 / \nu}, \tag{2}$$

where τ is a cooling age or Al-in-Hb exhumation value and ν is the degrees of freedom. The units of τ are both time (Ma) and length (km), which gives some weight to cooling ages over total exhumation values. For each inverse, we run approximately 1000 forward models (give or take 24) on a high-performance cluster computer. We then run an additional 1000 forward models in order to verify convergence and more fully explore the parameter space.

We interpret the results in terms of Bayesian posterior probability, which measures the likelihood that a given value of a parameter is the true value in the context of available data and any prior information (Sivia and Skilling, 2006). Posterior probability is better for estimating topographic parameters than a best-fit value with Gaussian error bars because of the non-linearity of the inverse and the complicated form of its

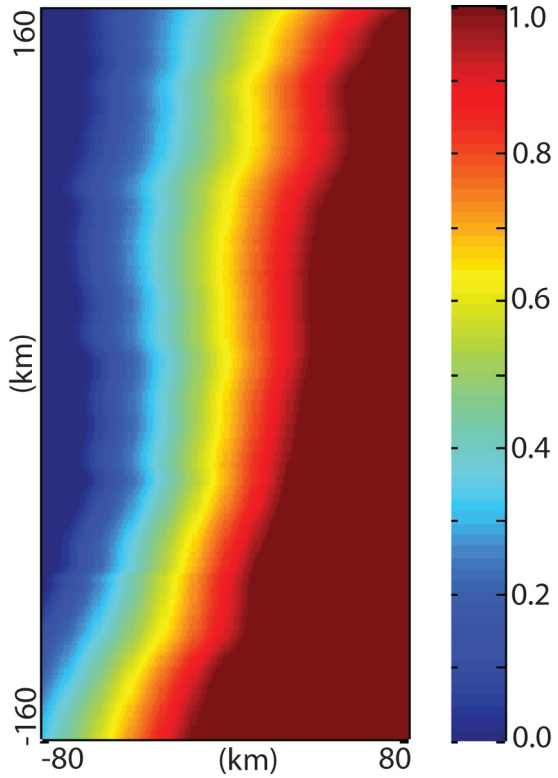

Fig. 5. Ramp function, as used to parameterize rock uplift. Map area is the same as the study area map (fig. 1). The ramp function has a value of 1 everywhere east of the Eastern Sierra Escarpment and a value of 0 west of the Great Valley lithologic transition (fig. 1). There is a linear gradient in between, with the slope determined by the local mean topographic slope. Rock uplift at any point in the model map area is given by the product of the ramp function at that point and the parameter *tectonicUplift*, plus the contribution from flexure.

error surface (see Tarantola, 2005). For example, an inverse using a least-squares approach will identify the best estimate of a single parameter as the value with the lowest misfit. However, the misfit is a function of all parameters. The set of parameters that yields the lowest misfit may include a single parameter value that is otherwise associated with large misfits. The posterior probability accounts for this problem. It is explicitly a function of all free parameters, but it may be integrated to examine the best estimates of one or more parameters independently of the others. The result of integrating a posterior probability function is called a marginal probability function. Either the posterior probability or a marginal probability may be used to describe confidence intervals in light of the available data (Sivia and Skilling, 2006).

After sampling the parameter space, the Neighborhood Algorithm constructs a robust approximation of the Bayesian posterior probability density function. For this calculation, we choose a standard form of the likelihood function and a uniform prior. Thus, the natural logarithm of the posterior probability value for each forward model is proportional to its chi-squared value:

$$\log P_j \cong -\frac{\nu}{2}\frac{\sigma_j^2}{\hat{\sigma}^2}, \tag{3}$$

where we use the standard deviation of the best fit forward model, $\hat{\sigma}$, as an estimate of the total uncertainty for the purpose of converting misfit values into chi-squared values. The Neighborhood Algorithm resamples and interpolates the individual probability values over the parameter space in order to estimate a continuous, multi-dimensional posterior probability density function. This function is then numerically integrated to find 1- and 2-dimensional marginal probabilities for each parameter or pair of parameters (Sambridge, 1999b). The narrowest interval of a 1-dimensional marginal probability that contains 68 percent of the probability can be viewed as a confidence interval for the given parameter. The 2-dimensional marginal probabilities help to demonstrate that the parameters are uncorrelated and therefore well chosen.

RESULTS

In total, we ran more than 16,000 forward models, including the runs for the 4 inverses described here. All of the inverse runs indicate that the Sierra Nevada started as a high mountain range, eroded to a minimum elevation in the mid- to late Cenozoic, and was subsequently uplifted to its present high elevation. The results show that the observed tilting of isochrones was achieved by a combination of initially high topography and subsequent rock uplift. Figure 6 shows the inverse results for our preferred parameterization scheme. This scheme has the best Bayesian Information Criterion score, which means that it has the lowest misfit value, weighted relative to the number of free parameters (Schwarz, 1978; Liddle, 2008). In this scheme, the model starts at 110 Ma. The state of the topography at this time (*time0*) is given by the parameters *rampElevation0* and *relief0*. Topography evolves toward a new state, given by *rampElevation1* and *relief1*, and achieves this state at the time given by *time1*. From *time1* until *time2* (0 Ma), the topography evolves to its present state. The parameters *tectonicUplift0* and *tectonicUplift1* give the tectonic component of rock uplift between successive topographic states. The eighth and final free parameter is the temperature at the base of the model, *basalTemp*. This parameter is fictive in the sense that it is only used to define the near-surface thermal gradient, rather than to actually resolve the temperature at the base of the crust. In all the inverses, the direct search method explores the range of plausible values for each parameter (see the plot axes; fig. 6). For example, the plausible range of topography is between zero and more than twice the present elevation—almost 9 km.

Figure 7 summarizes the results of several alternate parameterization schemes. These results support several important choices, including the model starting time and the complexity of the topographic evolution. In order to evaluate the best number of topographic states, we ran inverses with one (fig. 7A), two (fig. 6), and three states (fig. 7C). The number of free parameters rapidly increases because each additional state requires two topographic parameters, one time parameter, and one rock uplift parameter. Despite fewer free parameters, the one-state topographic evolution has by far the largest Bayesian Information Criterion score, indicating that the topographic evolution of the Sierra Nevada was not monotonic. In order to evaluate the best model start time, we ran inverses beginning near the start of Sierra Nevada plutonism (110 Ma; fig. 6) and near the end of plutonism (90 Ma, fig. 7B). The Bayesian Information Criterion scores favor the earlier model starting time (*time0*), although the results of both runs are similar.

The initial elevation of the Sierra Nevada was as high or higher than the modern elevation. In the preferred parameterization scheme, the parameter *relief0* is a modest fraction of the modern value, but the mean topographic surface, *rampElevation0* is almost twice the modern value (fig. 6). Taken together, these results indicate that the peaks of the Cretaceous Sierra Nevada were 5 to 6 km above sea level (fig. 8). All of the alternate parameterization schemes favor similarly high initial topography and low

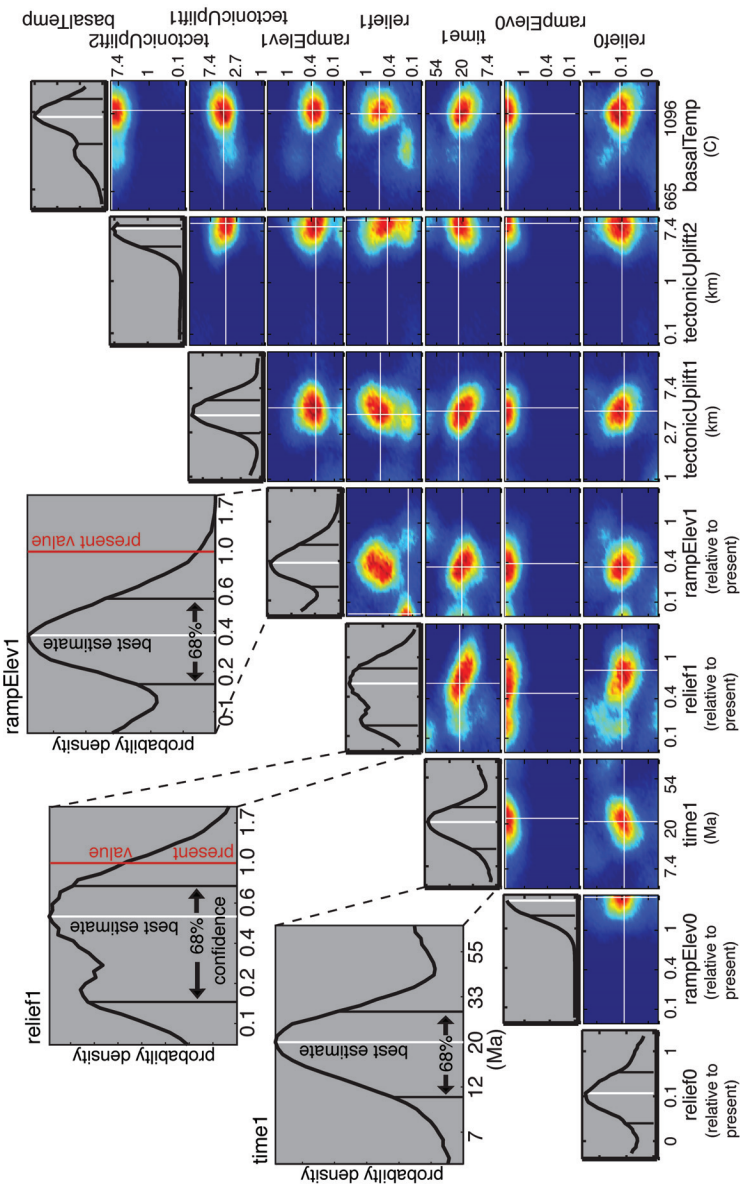

Fig. 6. Model inverse results in terms of 1- and 2-dimensional marginal probability distributions. The 1-dimensional distributions are on the diagonal and provide a clear choice for the best estimate, while the 2-dimensional distributions are on the off-diagonals and show that parameters have little covariance. Three 1-dimensional distributions are expanded because they are directly relevant to Cenozoic surface uplift (see text for discussion). The inverse features eight free parameters. The first five parameters, *relief0, rampElev0, time1, relief1, rampElev1*, describe the topographic evolution. The parameters *tectonicUplift0* and *tectonicUplift1* describe the rock velocities in the intervals between *time0* to *time1* and *time1* to *time2*, respectively, in terms of maximum rock displacement. The last parameter, *basalTemp*, describes the temperature at the base of the model, at 50 km depth, for the duration. Note that the ranges of values allowed for the inverse were bounded by reasonable values, as shown. In particular, the maximum elevation was fixed at 9 km. Also note that the magnitudes of each distribution have a unique scaling because all probability densities are relative and the likelihood method only provides probability up to an unknown scale factor.

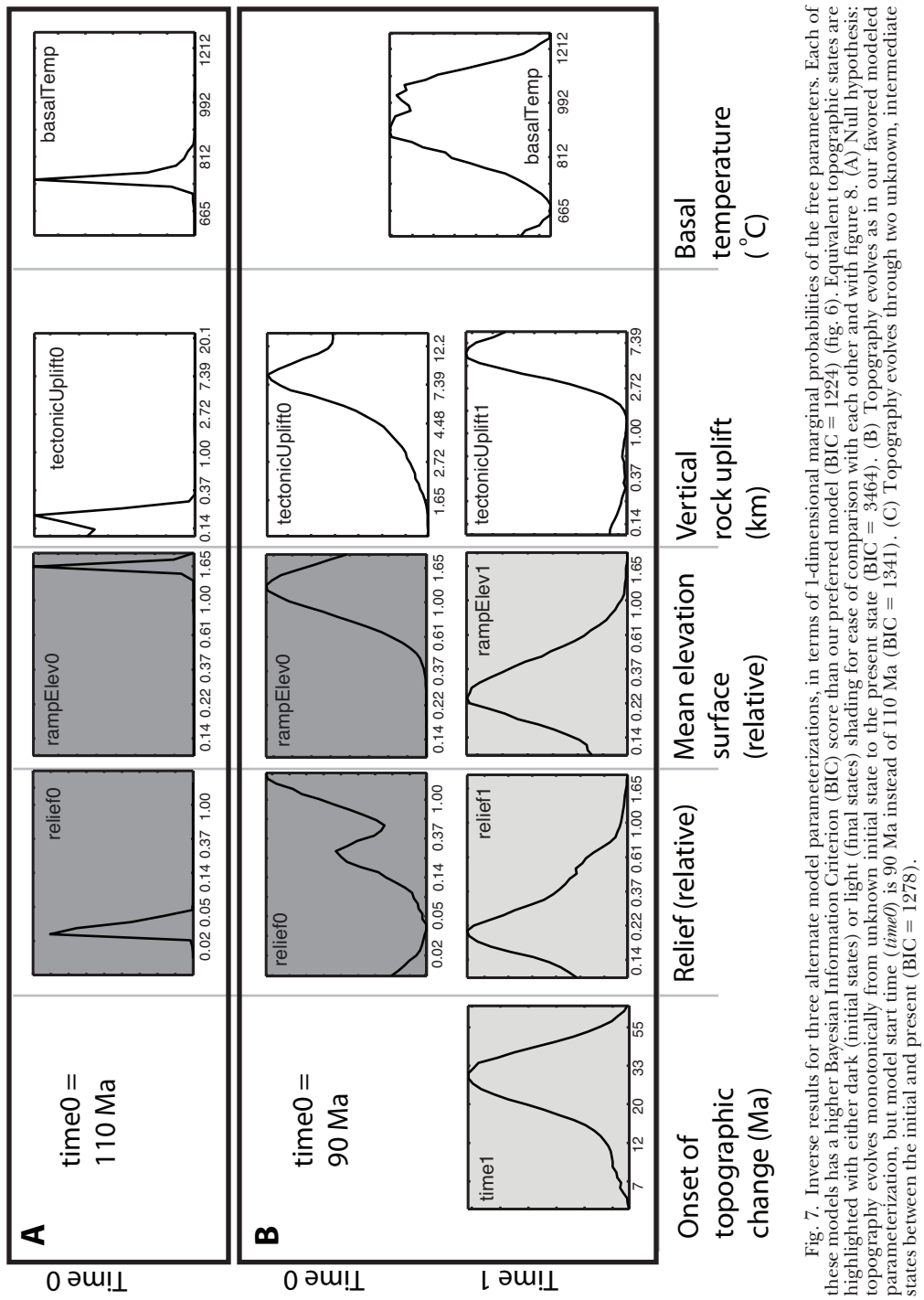

Fig. 7. Inverse results for three alternate model parameterizations, in terms of 1-dimensional marginal probabilities of the free parameters. Each of these models has a higher Bayesian Information Criterion (BIC) score than our preferred model (BIC = 1224) (fig. 6). Equivalent topographic states are highlighted with either dark (initial states) or light (final states) shading for ease of comparison with each other and with figure 8. (A) Null hypothesis: topography evolves monotonically from unknown initial state to the present state (BIC = 3464). (B) Topography evolves as in our favored modeled parameterization, but model start time (*time0*) is 90 Ma instead of 110 Ma (BIC = 1341). (C) Topography evolves through two unknown, intermediate states between the initial and present (BIC = 1278).

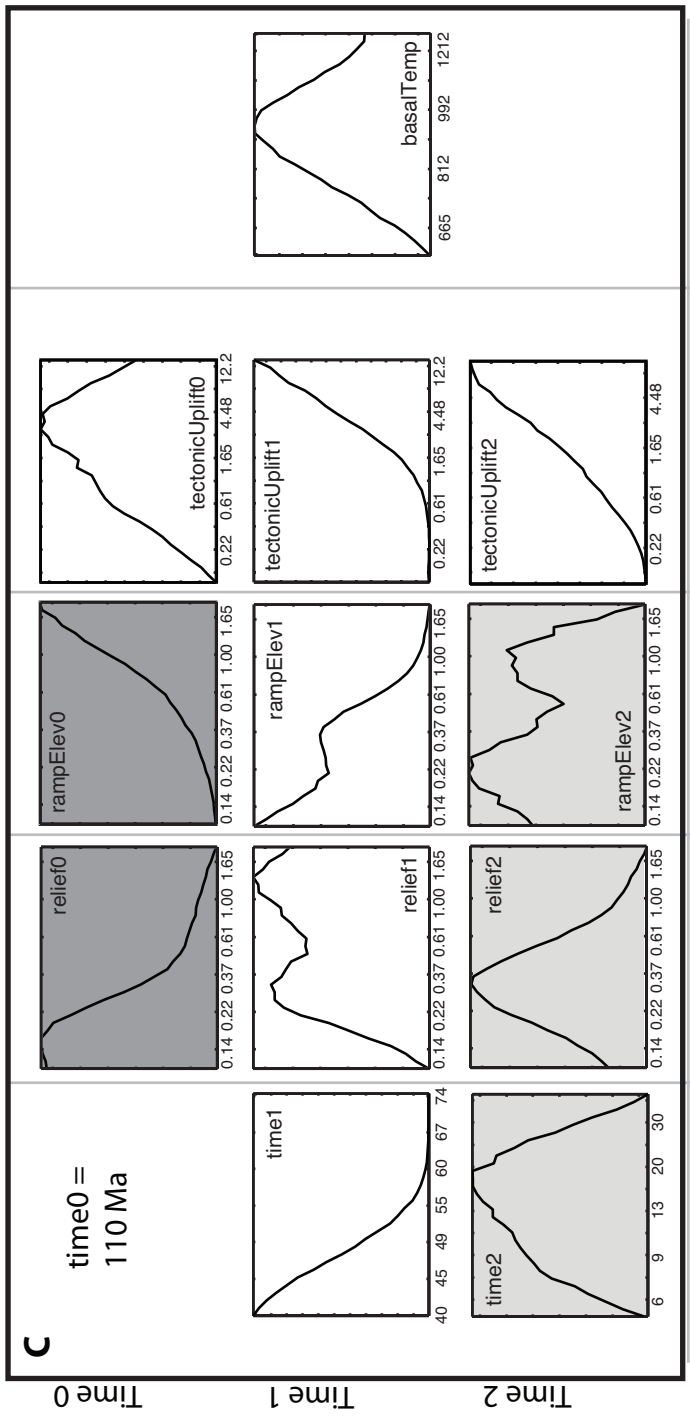

Fig. 7 (continued)

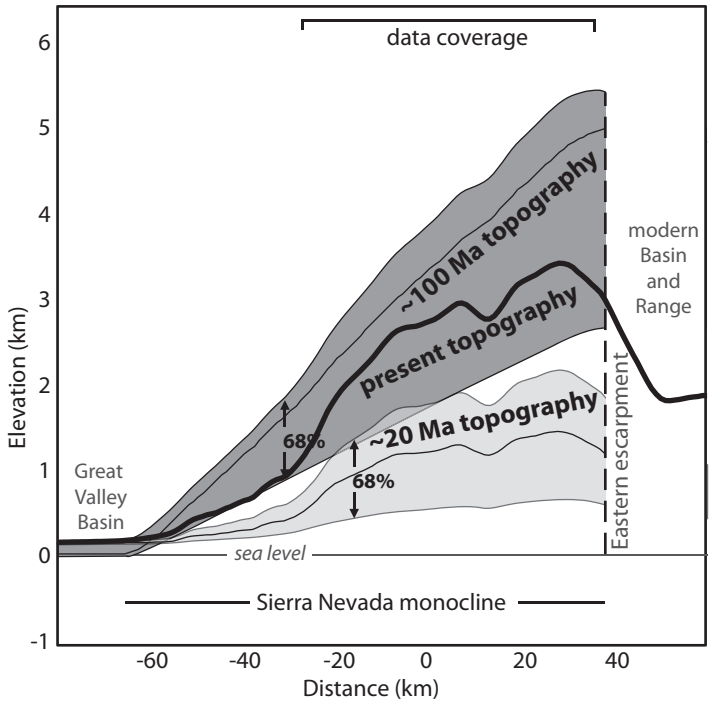

Fig. 8. Cross-section showing past and present elevations of the southern Sierra Nevada as constrained by thermochronology. Elevations are tied to the Great Valley, which was near sea level since the Late Cretaceous (see text for discussion). Confidence intervals at 68% are taken from the 1-dimensional marginal probability distributions (fig. 6). A time-lapse animation of this figure is available for download in the online supplement (http://earth.geology.yale.edu/~ajs/SupplementaryData/2012/03McPhillipsMovie.avi).

relief (fig. 7), although in one case the marginal probability distribution for *relief0* is bimodal (fig. 7B).

The Sierra Nevada reaches its minimum elevation at the intermediate topographic state (*time1*). Although the topography is lower at this time, it is still substantial (fig. 8). The best estimate of relief, *relief1*, is 51 percent of the modern value (fig. 6). The mean topographic surface, *rampElevation1*, is most likely 35 percent of the modern. Both parameters are lower than the modern values within at least 68 percent confidence. Among the alternate parameterization schemes that permit intermediate states, all show elevations that are lower than the modern value. In fact, the alternate parameterizations generally favor intermediate elevations that are much lower—the peak marginal probabilities are generally around 20 percent of the modern for both topographic parameters (fig. 7).

The topographic minimum occurs in the mid- to late Cenozoic. The best estimate for the timing of the intermediate topographic state (*time1*) is 20 Ma (fig. 6). The alternate parameterization scheme with two intermediate states shows a topographic minimum at 17 Ma (*time2*; fig. 7C). The alternate with one intermediate state shows a minimum at 26 Ma (*time1*; fig. 7B). Both of these values fall within the 68 percent confidence intervals of the best estimate, which is between 30 and 10 Ma (fig. 6).

In order to examine the details of the topographic evolution we rely on the forward model run using the best estimate values of all parameters (fig. 9). For most of the model run, erosion rates are predicted to be in the range of 0.03 to 0.08 km/Ma. These rates are in agreement with those estimated from apatite (U-Th)/He age-

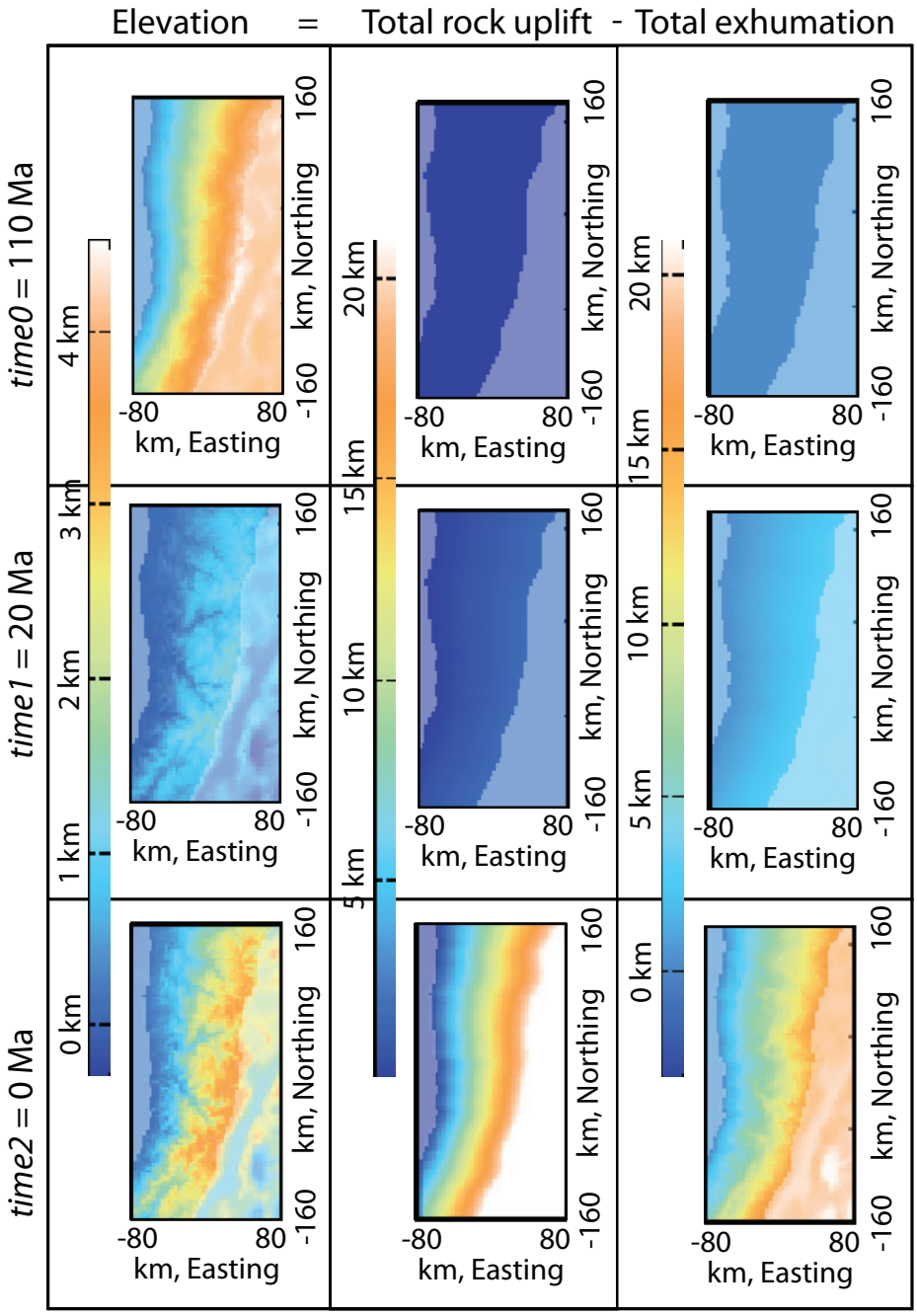

Fig. 9. Forward model results for the best estimate parameter values. Exhumation is defined as the sum of surface and rock offset and is accomplished by erosion. Surface offset is the sum of the parameters *relief* and *rampElev*. Rock uplift is given by the parameter *tectonicUplift* plus any flexural adjustments (fig. 6). The grid shows these sums graphically at each topographic state. The difference in the transparency of the color scheme shows the map area where we have elevation control (that is, between the eastern boundary of the Great Valley and the Eastern Escarpment).

elevation relationships (House and others, 1997; House and others, 2001; McPhillips and Brandon, 2010). After *time1*, stream incision must increase in order to cut the present relief. The peak exhumation rates in large river valleys approaches 0.3 km/Ma during this interval. This value is comparable to the maximum incision rate documented by cosmogenic nuclides in the Kings River canyon during the Pliocene (Stock and others, 2005). Although the peak exhumation rates in the model are greater than the estimates from age-elevation relationships, the two values are likely consistent. The inverse predicts that incision began around 20 Ma, well after even the younger cooling ages were set. As a result, age-elevation estimates, which measure erosion rates during the interval between the oldest and youngest cooling ages, are not an accurate measure of more recent rates. Total exhumation rates are in good agreement with Al-in-hornblende barometry measurements of 8 to 10 km (Ague and Brimhall, 1988).

The overall quality of the fit is best judged in terms of the residuals of the observed cooling ages and barometry measurements. The standard deviation of all the residuals is 9.1, which is greater than the average analytical error by a factor of 3. In terms of the R^2 statistic, this fit corresponds to a 37 percent improvement over the mean (U-Th)/He age. The empirical isochrone fit of McPhillips and Brandon (2010) has an R^2 value of 68 percent for the same data. The thermal-kinematic model treats the full physics of the problem with a highly simplified version of the topographic evolution. The residuals show little systematic variation. We measure this in two ways. First, we apply the Von Neumann Rank Ratio test (Bartels, 1982) to the residuals, in projections parallel to both isochrone strike and dip. These tests show no significant systematic variation in either direction. (Note that a model without dipping isochrones would fail this test.) Second, we address the potential for 2-dimensional spatial autocorrelation using a variogram, which plots variance of each pair of residuals as a function of distance (fig. 10). The uniform scatter of points on the variogram is as expected for a case without spatial autocorrelation (Wackernagel, 2003). The lack of correlation among residuals indicates that the model fit captures the essence of the topographic evolution.

DISCUSSION

Topography

Our analysis supports the idea, proposed by Braun (2003), that the evolution of paleotopography can be represented using factors that scale the paleotopography relative to the modern topography. There is no guarantee that this approach will work in other areas, but it does provide a useful first step in relating geologic and thermochronologic data to the evolution of ancient topography. Our approach is motivated by the work of House and others (1997, 1998, 2001), who use nearly the same cooling age data to argue for late Cretaceous topographic relief aligned with, but exceeding, modern river canyons. However, our comprehensive analysis shows very little local relief in the Cretaceous. The steady state, 2-dimensional estimates of House and others (1997, 1998, 2001) are evidently insufficient to capture the evolution of local relief, perhaps in part due to the sampling strategy (Braun, 2002). While we do not preclude Cretaceous transverse drainages, we find no evidence for local relief at the scale suggested by House and others (1997, 1998, 2001) to be aligned with modern canyons. For the mid-Cenozoic Sierra Nevada, our results are in agreement with more sophisticated investigations into stream morphology. Clark and others (2005) identify two uplift and incision events since 32 Ma. Pre-Pliocene relief documented by Stock and others (2004, 2005) was likely incised beginning at around this time.

This inverse analysis is limited to data in the southern Sierra Nevada, between Mt. Whitney and the Merced River. Areas to the south and north may have different histories. However, the character of isochrones in the south implies that the northern

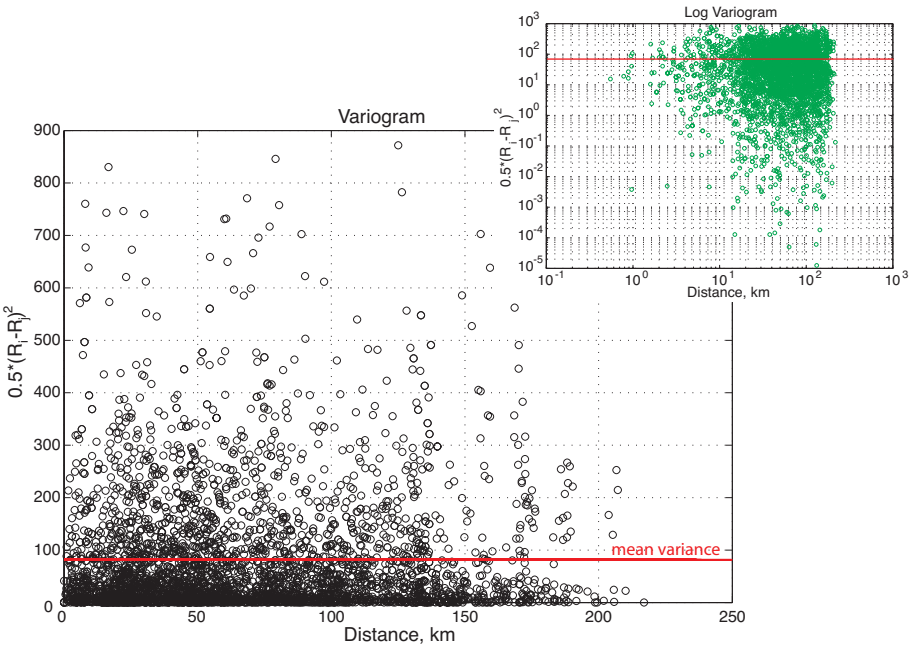

Fig. 10. Variogram showing little or no spatial correlation among model residuals. The variance for each pair of model residuals is plotted against the distance between the pair. In the case of spatial autocorrelation, we would expect to see a relationship between these variables, typically an inverse distance-squared relationship, but no such relationship is evident. Furthermore, Von Neumann rank-ratio tests show no statistically significant autocorrelation along either of the principal axes of the data (see text).

Sierra has similar history. McPhillips and Brandon (2010) show that the isochrones in the south have an orientation that matches the dipping strata in the north that were originally used to identify tilting (for example Unruh, 1991; Wakabayashi and Sawyer, 2001). The isochrone dip of 3.4° is in particularly good agreement with the dip of the Eocene Ione Formation in the north (Unruh, 1991). Furthermore, the residuals from fitting the isochrones to the actual cooling ages show no systematic trends from north to south (McPhillips and Brandon, 2010). Absent major structures separating the northern and southern Sierra, the common orientations suggest a single tilting event beginning sometime after the mid-Tertiary.

The timing and extent of Cenozoic surface uplift also provide clues about the cause. Our analysis supports the onset of surface uplift throughout the southern Sierra Nevada between 30 and 10 Ma, culminating in about 2 km of peak uplift. By 30 Ma, Farallon slab subduction was essentially complete (Atwater and Stocker, 1988), requiring an alternate driver for more recent uplift. Our analysis demonstrates that an isostatic response to valley incision, as proposed by Small and Anderson (1995), cannot account for recent uplift—a significant amount of tectonic rock uplift is required to produce the observed tilting of isochrones. The more likely drivers include the removal of dense lower lithosphere (Ducea and Saleeby, 1996; Lee and others, 2001; Zandt and others, 2004), isostasy related to normal faulting (Thompson and Parsons, 2009), and dynamic topography (Mitrovica and others, 1989; Lowry and others, 2000; Moucha and others, 2009; Liu and Gurnis, 2010). Among these, only dynamic topography was active prior to 10 Ma; xenoliths record a thick crust and lithosphere

(Ducea and Saleeby, 1996; Lee and others, 2001), and Basin and Range extension had not yet reached the Eastern Sierra Escarpment (Bachman, 1978). However, dynamic topography does not provide a satisfying explanation. The mantle buoyancy that is invoked for the uplift of the Colorado Plateau is the result of convection deep in the asthenosphere (Mitrovica and others, 1989; Moucha and others, 2009; Liu and others, 2010). Dynamic topography of this sort is expressed over long wavelengths, usually many hundreds of kilometers. The fact that Great Valley boundary has remained at sea level, less than 100 km from the crest of the Sierra Nevada, implies a limited role for dynamic topography. Geophysical (Wernicke and others, 1996; Zandt and others, 2004) and geochemical (Ducea and Saleeby, 1996; Lee and others, 2001) evidence document the removal of dense lower lithosphere in the southern Sierra Nevada, which likely had some effect on surface elevation (Jones and others, 2004). However, the presence of a thick crust in the northern Sierra Nevada (Frassetto and others, 2010) suggests that this mechanism is not responsible for tilting observed in the north (for example, Wakabayashi and Sawyer, 2001). In contrast, an isostatic response to extensional faulting along the Eastern Sierra Escarpment and Walker Lane could drive a maximum of 1 km of surface uplift and tilting along the length of the range (Thompson and Parsons, 2009). Therefore, we favor a combination of lower lithosphere removal and extension-driven isostasy as a main causes of uplift in the southern Sierra Nevada, with a smaller contribution from dynamic topography in the Miocene.

Modeling with Pecube

The model Pecube is a powerful and flexible tool, but it requires some modification to be useful for measuring paleoelevation. Notably, Pecube always requires some prior constraint on rock velocity, typically in terms of specific displacements along faults or with the assumption of a uniform vertical velocity field (Braun, 2003). The isochrone conceptual model provides a convenient means of distinguishing a uniform velocity field, which yields flat structures, from a more complex field, which yields tilted or complex structures. It is important to test for these structures before running Pecube in most scenarios. Our results demonstrate the utility of this approach for arriving at a viable functional form of rock uplift, thereby permitting paleoelevation measurements.

In order to measure paleoelevation specifically, Pecube (or any thermal-kinematic model) must include a datum such as the Great Valley paleoshoreline. For our analysis, this boundary serves a double purpose. First, it fixes the thermal field with respect to sea level. Cooling ages are capable of measuring relief change at many scales, due to the influence of relief on the closure surface (Mancktelow and Grasemann, 1997). By including the shoreline in the model runs, we are able to measure relief change at a very large spatial scale that is linked to a sea-level datum. Decomposing topography into the mean surface and relief allows topography to evolve independently of small-scale relief. This is particularly important for the initial state of the model, when valley relief could have been oriented differently than at present. Second, the Great Valley shoreline is a datum for rock velocity. Because it persisted near the erosion-aggradation boundary, this boundary provides a zero-velocity line that is important for developing the rock uplift parameterization.

It may seem curious that (U-Th)/He cooling ages ranging between 85 and 23 Ma can resolve paleoelevation during the entire period since approximately 100 Ma. The principal constraint on recent (late Cenozoic) incision is the range of exposed cooling ages. Relief must have been cut relatively recently in order to expose such a large range of ages at the surface. If relief were long-lived, the closure isotherm would warp according to the surface boundary condition, and the ages exposed in ridges and valleys would eventually approach a common value. The data place direct constraints on erosion and uplift during the interval of closure, from 85 to 23 Ma. Prior to closure,

the topography must define an initial condition that agrees with the Al-in-Hb total exhumation data (Ague and Brimhall, 1988), limited fission track data (Dumitru, 1990), and the subsequent topographic evolution.

CONCLUSIONS

In conclusion, we emphasize the geological scenario revealed by the inversion of low-temperature thermochronology. These paleotopography results are broadly consistent with other observations and potentially reconcile conflicting interpretations. The southern Sierra Nevada was high in the Late Cretaceous, declined through most of the Cenozoic, and began to grow again early in the Miocene. The onset of surface uplift and incision between 30 to 10 Ma is an especially robust result, which is common to virtually all choices of parameterization. Immediately prior to this event, the southern Sierra Nevada was at a lower elevation than any time before or since. Renewed surface uplift was likely driven by several processes, perhaps beginning with a small contribution from dynamic topography in the Miocene and then bolstered by larger contributions from lower lithosphere removal and the isostatic response to normal faulting.

Although our analysis does not resolve whether the topography of the northern Sierra Nevada was also uplifted in the late Cenozoic, it seems likely that it was, in light of the similar tilt of isochrones in the south and sedimentary and geomorphic surfaces in the north. According to our analysis, high, but decaying, topography would have persisted well into the Tertiary. Our results also support the idea of a high-elevation region to the east of the Sierra Nevada during Cretaceous time. It remains unclear whether this upland region had low relief, like the modern Andean Altiplano (DeCelles, 2004), or whether it had higher relief, like the modern Puna Plateau. Recent stable isotope work, interpreted to suggest a complex and diachronous history of uplift, may be consistent with large local relief in the surrounding Cordillera (for example, Mix and others, 2011; Chamberlain and others, 2012). Our study in the southern Sierra Nevada illustrates the importance of considering both local relief and long-wavelength topography.

ACKNOWLEDGMENTS

The authors thank Jean Braun, Frederic Herman, and David Shuster for discussions about thermochronologic data and the NA and Pecube inverse, and Brian Dobbins for assistance with cluster computing. Stephen Graham and Andreas Mulch provided constructive reviews. This work was supported in part by the facilities and staff of the Yale University Faculty of Arts and Sciences High Performance Computing Center.

APPENDIX

Supplementary information is available online: http://earth.geology.yale.edu/~ajs/SupplementaryData/2012/03McPhillipsMovie.avi

REFERENCES

Ague, J. J., and Brimhall, G. H., 1988, Magmatic arc asymmetry and distribution of anomalous plutonic belts in the batholiths of California: Effects of assimilation, crustal thickness, and depth of crystallization: Geological Society of America Bulletin, v. 100, n. 6, p. 912–927, http://dx.doi.org/10.1130/0016-7606(1988)100⟨0912:MAAADO⟩2.3.CO;2

Armstrong, R. L., 1982, Cordilleran metamorphic core complexes—from Arizona to southern Canada: Annual Reviews of Earth and Planetary Sciences, v. 10, p. 129–154, http://dx.doi.org/10.1146/annurev.ea.10.050182.001021

Atwater, T., and Stock, J., 1988, Pacific–North America plate tectonics of the Neogene Southwestern United States: An Update: International Geological Review, v. 40, n. 5, p. 375–402, http://dx.doi.org/10.1080/00206819809465216

Bachman, S. B., 1978, Pliocene-Pleistocene break-up of the Sierra Nevada-White-Inyo Mountains block and

formation of Owens Valley: Geology, v. 6, n. 8, p. 461–463, http://dx.doi.org/10.1130/0091-7613(1978)6⟨461:PBOTSN⟩2.0.CO;2
Bartels, R., 1982, The rank version of Von Neumann's ratio test for randomness: Journal of the American Statistical Association, v. 77, n. 377, p. 40–46, http://dx.doi.org/10.2307/2287767
Bartow, J., A., 1991, The Cenozoic evolution of the San Joaquin Valley, California: U.S. Geological Survey Professional Paper 1501, 40 p.
Benz, H. M., and Zandt, G., 1993, Teleseismic tomography: Lithospheric structure of the San Andreas Fault system in northern and central California, *in* Iyer, H. M., and Hirahara, K., editors, Seismic tomography: Theory and practice: New York, New York, Chapman and Hall, p. 440–465.
Brady, R. J., Ducea, M. N., Kidder, S. B., and Saleeby, J. B., 2006, The distribution of radiogenic heat production as a function of depth in the Sierra Nevada batholith, California: Lithos, v. 86, p. 229–244, http://dx.doi.org/10.1016/j.lithos.2005.06.003
Braun, J., 2002, Estimating exhumation rate and relief evolution by spectral analysis of age-elevation datasets: Terra Nova, v. 14, n. 3, p. 210–214, http://dx.doi.org/10.1046/j.1365-3121.2002.00409.x
——— 2003, Pecube: a new finite-element code to solve the 3D heat transport equation including the effects of a time-varying, finite amplitude surface topography: Computers and Geoscience, v. 29, n. 6, p. 787–794, http://dx.doi.org/10.1016/S0098-3004(03)00052-9
Cassel, E. J., Graham, S. A., and Chamberlain, C. P., 2009, Cenozoic tectonic and topographic evolution of the northern Sierra Nevada, California, through stable isotope paleoaltimetry in volcanic glass: Geology, v. 37, n. 6, p. 547–550, http://dx.doi.org/10.1130/G25572A.1
Cassel E. J., Graham, S. A., Chamberlain, C. P., and Henry, C., 2012, Early Cenozoic Topography, Morphology, and Tectonics of the Northern Sierra Nevada and Western Basin and Range: Geosphere, v. 8, http://dx.doi.org/10.1130/GES00671
Cecil, M. R., Ducea, M. N., Reiners, P., Gehrels, G., Mulch, A., Allen, C., and Campbell, I., 2010, Provenance of Eocene river sediments from the central northern Sierra Nevada and implications for paleotopography: Tectonics, v. 29, TC6010, http://dx.doi.org/10.1029/2010TC002717
Chamberlain, C. P., Mix, H. T., Mulch, A., Hren, M. T., Kent-Corson, M. L., Davis, S. J., Horton, T. W., and Graham, S. A., 2012, The Cenozoic climatic and topographic evolution of the Western North American Cordillera: American Journal of Science, v. 312, p. 213–262, http://dx.doi.org/10.2475/02.2012.05.
Chase, C. G., and Wallace, T. C., 1986, Uplift of the Sierra Nevada of California: Geology, v. 14, n. 9, p. 730–733, http://dx.doi.org/10.1130/0091-7613(1986)14⟨730:UOTSNO⟩2.0.CO;2
Chen, J. H., and Moore, J. G., 1982, Uranium-lead isotopic ages from the Sierra Nevada Batholith, California: Journal of Geophysical Research, v. 87, n. B6, p. 4761–4784, http://dx.doi.org/10.1029/JB087iB06p04761
Cherniak, D. J., Watson, E. B., and Thomas, J. B., 2009, Diffusion of helium in zircon and apatite: Chemical Geology, v. 268, n. 1–2, p. 155–66, http://dx.doi.org/10.1016/j.chemgeo.2009.08.011
Cherven, V. B., 1983, A delta-slope-submarine fan model for Maestrichtian part of Great Valley sequence, Sacramento and San Joaquin Basins, California: AAPG Bulletin, v. 67, n. 5, p. 772–816.
Christensen, N. I., and Mooney, W. D., 1995, Seismic velocity structure and composition of the continental crust: A global view: Journal of Geophysical Research, v. 100, n. B6, p. 9761–9788, http://dx.doi.org/10.1029/95JB00259
Clark, M. K., Maheo, G., Saleeby, J., and Farley, K. A., 2005, The non-equilibrium landscape of the southern Sierra Nevada, California: GSA Today, v. 15, n. 9, p. 4–10, http://dx.doi.org/10:1130/1052-5173(2005)015⟨4:TNELOT⟩2.0.CO;2
Coney, P. J., and Harms, T. A., 1984, Cordilleran metamorphic core complexes: Cenozoic extensional relics of Mesozoic compression: Geology, v. 12, n. 9, p. 550–554, http://dx.doi.org/10.1130/0091-7613(1984)12⟨550:CMCCCE⟩2.0.CO;2
Cowan, D. S., Brandon, M. T., and Garver, J. I., 1997, Geologic tests of hypotheses for large coastwise Displacements—A critique illustrated by the Baja British Columbia controversy: American Journal of Science, v. 297, n. 2, p. 117–173, http://dx.doi.org/10.2475/ajs.297.2.117
Crowley, B. E., Koch, P. L., and Davis, D. B., 2008, Stable isotope constraints on the elevation history of the Sierra Nevada Mountains, California: Geological Society of America Bulletin, v. 120, n. 5–6, p. 588–598, http://dx.doi.org/10.1130/B26254.1
DeCelles, P. G., 2004, Late Jurassic to Eocene evolution of the Cordilleran thrust belt and foreland basin system, western U.S.A.: American Journal of Science, v. 304, n. 2, p. 105–168, http://dx.doi.org/10.2475/ajs.304.2.105
Dickinson, W. R., and Snyder, W. S., 1979, Geometry of subducted slabs related to San Andreas transform: Journal of Geology, v. 87, p. 609–627, http://www.jstor.org/stable/30068692
Dickinson, W. R., Ingersoll, R. V., and Graham, S. A., 1979, Paleogene sediment dispersal and paleotectonics in northern California: Geological Society of America Bulletin, v. 90, n. 10, p. 1458–1528, http://dx.doi.org/10.1130/GSAB-P2-90-1458
Dixon, T. H., Miller, M., Farina, F., Wang, H., and Johnson, D., 2000, Present-day motion of the Sierra Nevada block and some tectonic implications for the Basin and Range province, North America Cordillera: Tectonics, v. 19, n. 1, p. 1–24, http://dx.doi.org/10.1029/1998TC001088
Dodson, M. H., 1973, Closure temperature in cooling geochronological and petrological systems: Contributions in Mineralogy and Petrology, v. 40, n. 3, p. 259–274, http://dx.doi.org/10.1007/BF00373790
Ducea, M. N., and Saleeby, J. B., 1996, Buoyancy sources for a large, unrooted mountain range, the Sierra Nevada, California: evidence from xenolith thermobarometry: Journal of Geophysical Research—Solid Earth, v. 101, n. B4, p. 8229–8244, http://dx.doi.org/10.1029/95JB03452
Dumitru, T. A., 1990, Subnormal Cenozoic geothermal gradients in the extinct Sierra Nevada magmatic arc: Consequences of Laramide and post-Laramide shallow-angle subduction: Journal of Geophysical Research, v. 95, n. B4, p. 4925–4941, http://dx.doi.org/10.1029/JB095iB04p04925

Ehlers, T. A., Chaudhri, T., Kumar, S., Fuller, C. W., Willett, S. D., Ketcham, R. A., Brandon, M. T., Belton, D. X., Kohn, B. P., Gleadow, A. J. W., Dunai, T. J., and Fu, F. Q., 2005, Computational tools for low-temperature thermochronometer interpretation, *in* Ehlers, T., and Reiners, P., editors, Low-Temperature Thermochronology: Techniques, Interpretations, Applications: Reviews in Mineralogy and Geochemistry, v. 58, p. 589–622, http://dx.doi.org/10.2138/rmg.2005.58.22

England, P., and Molnar, P., 1990, Surface uplift, uplift of rocks, and exhumation of rocks: Geology, v. 18, n. 12, p. 1173–1177, http://dx.doi.org/10.1130/0091-7613(1990)018⟨1173:SUUORA⟩2.3.CO;2

Evernden, J. F., and Kistler, R. W., 1970, Chronology of emplacement of Mesozoic batholithic complexes in California and western Nevada: U.S. Geological Survey Professional Paper 623, 42 p.

Farley, K. A., 2000, Helium diffusion from apatite: general behavior as illustrated by Durango fluorapatite: Journal of Geophysical Research, v. 105, n. B2, p. 2903–2914, http://dx.doi.org/10.1029/1999JB900348

Flowers, R. M., Ketcham, R. A., Shuster, D. L., and Farley, K. A., 2009, Apatite (U-Th)/He thermochronometry using a radiation damage accumulation and annealing model: Geochimica et Cosmochimica Acta, v. 73, n. 8, p. 2347–2365, http://dx.doi.org/10.1016/j.gca.2009.01.015

Frassetto, A., Zandt, G., Gilbert, H., Owens, T. J., and Jones, C. H., 2010, Improved imaging with phase-weighted common conversion point stacks of receiver functions: Geophysical Journal International, v. 182, n. 1, p. 368–374, http://dx.doi.org/10.1111/j.1365-246X.2010.04617.x

Gautheron, C., Tassan-Got, L., Barbarand, J., and Pagel, M., 2009, Effect of alpha-damage annealing on apatite (U-Th)/He thermochronology: Chemical Geology, v. 266, n. 34, p. 157–170, http://dx.doi.org/10.1016/j.chemgeo.2009.06.001

Göğüs, O. H., and Pysklywec, R. N., 2008, Near-surface diagnostics of dripping or delaminating lithosphere: Journal of Geophysical Research, v. 113, n. B11404, http://dx.doi.org/10.1029/2007JB005123

Granger, D. E., and Stock, G. M., 2004, Using cave deposits as geologic tiltmeters: Application to postglacial rebound of the Sierra Nevada: Journal of Geophysical Research, v. 31, L22501, http://dx.doi.org/10.1029/2004GL021403

Herman, F., Copeland, P., Avouac, J-P., Bollinger, L., Mahéo, G., Le Fort, P., Rai, S. M., Foster, D., Pêcher, A., Stüwe, K., and Henry, P., 2010. Exhumation, crustal deformation and thermal structure of the Nepal Himalaya derived from the inversion of thermochronological and thermobarometric data and modeling of the topography: Journal of Geophysical Research, Solid Earth, v. 115, B06407, http://dx.doi.org/10.1029/2008JB006126

House, M. A., Wernicke, B. P., Farley, K. A., and Dumitru, T. A., 1997, Cenozoic thermal evolution of the central Sierra Nevada, California, from (U-Th)/He thermochronometry: Earth and Planetary Science Letters, v. 151, n. 3–4, p. 167–179, http://dx.doi.org/10.1016/S0012-821X(97)81846-8

House, M. A., Wernicke, B. P., and Farley, K. A., 1998, Dating topography of the Sierra Nevada, California, using apatite (U-Th)/He ages: Nature, v. 396, p. 66–69, http://dx.doi.org/10.1038/23926

——— 2001, Paleo-geomorphology of the Sierra Nevada, California, from (U-Th)/He ages in apatite: American Journal of Science, v. 301, p. 77–102, http://dx.doi.org/10.2475/ajs.301.2.77

Houseman, G. A., McKenzie, D. P., and Molnar, P., 1981, Convective instability of a thickened boundary layer and its relevance for the thermal evolution of continental convergent belts: Journal of Geophysical Research, v. 86, n. B7, p. 6115–6132, http://dx.doi.org/10.1029/JB086iB07p06115

Hren, M. T., Pagani, M., Erwin, D. W., and Brandon, M., 2010, Biomarker reconstruction of the early Eocene paleotopography and paleoclimate of the northern Sierra Nevada: Geology, v. 38, n. 1, p. 7–10, http://dx.doi.org/10.1130/G30215.1

Huang, J., and Turcotte, D. L., 1990, Fractal image analysis: application to the topography of Oregon and synthetic images: Journal of the Optical Society of America A, v. 7, n. 6, p. 1124–1130, http://dx.doi.org/10.1364/JOSAA.7.001124

Huber, N. K., 1981, Amount and timing of Late Cenozoic uplift and tilt of the Central Sierra Nevada, California—Evidence from the Upper San Joaquin River basin: U.S. Geological Survey Professional Paper 1197, 28 p.

Ingersoll, R. V., 1979, Evolution of the Late Cretaceous forearc basin, northern and central California: Geological Society of America Bulletin, v. 90, n. 9, p. 813–826, http://dx.doi.org/10.1130/0016-7606(1979)90⟨813:EOTLCF⟩2.0.CO;2

Jones, C. H., Farmer, G. L., and Unruh, J., 2004, Tectonics of Pliocene removal of lithosphere of the Sierra Nevada, California: Geological Society of America Bulletin, v. 116, p. 1408–1422, http://dx.doi.org/10.1130/B25397.1

Lachenbruch, A. H., and Sass, J. H., 1977, Heat flow in the United States and the thermal regime of the crust, *in* Heacock, J. G., Keller, G. V., Oliver, J. E., and Simmons, G., editors, The Earth's Crust: Geophysical Monographs Series 20, p. 626–675, http://dx.doi.org/10.1029/GM020p0626

Le Pourhiet, L., Gurnis, M., and Saleeby, J., 2006, Mantle instability beneath the Sierra Nevada Mountains in California and Death Valley extension: Earth and Planetary Science Letters, v. 251, p. 104–119, http://dx.doi.org/10.1016/j.epsl.2006.08.028

LeConte, J., 1886, A post-Tertiary elevation of the Sierra Nevada shown by the river beds: American Journal of Science, Third Series, v. 32, n. 189, p. 167–181.

Lee, C., Rudnick, R. L., and Brimhall, G. H., Jr., 2001, Deep lithospheric dynamics beneath the Sierra Nevada during the Mesozoic and Cenozoic as inferred from xenolith petrology: Geochemistry Geophysics Geosystems, v. 2, n. 12, http://dx.doi.org/10.1029/2001GC000152

Leopold, L. B., and Bull, W. B., 1979. Base level, aggradation, and grade: Proceedings of the American Philosophical Society, v. 123, n. 3, p. 168–202, http://www.jstor.org/stable/986220

Liddle, A. R., 2008, Information criteria for astrophysical model selection: Monthly Notices of the Royal Astronomical Society: Letters, v. 377, n. 1, p. L74–L78, http://dx.doi.org/10.1111/j.1745-3933.2007.00306.x

Lindgren, W., 1911, The Tertiary gravels of the Sierra Nevada of California: U.S. Geological Survey Professional Paper 73, 226 p.
Liu, L., and Gurnis, M., 2010, Dynamic subsidence and uplift of the Colorado Plateau: Geology, v. 38, n. 7, p. 663–666, http://dx.doi.org/10.1130/G30624.1
Lowry, A. R., Ribe, N. M., and Smith, R. B., 2000, Dynamic elevation of the Cordillera, western United States: Journal of Geophysical Research, v. 105, n. B10, p. 23,371–23,390, http://dx.doi.org/10.1029/2000JB900182
Maheo, G., Saleeby, J., Saleeby, Z., and Farley, K. A., 2009, Tectonic control on the southern Sierra Nevada topography, California: Tectonics, v. 28, TC6006, http://dx.doi.org/10.1029/2008TC002340
Mancktelow, N. S., and Grasemann, B., 1997, Time-dependent effects of heat advection and topography on cooling histories during erosion: Tectonophysics, v. 270, n. 3–4, p. 167–195, http://dx.doi.org/10.1016/S0040-1951(96)00279-X
McPhillips, D., and Brandon, M. T., 2010, Using tracer thermochronology to measure modern relief change in the Sierra Nevada, California: Earth and Planetary Science Letters, v. 296, n. 3–4, p. 373–383, http://dx.doi.org/10.1016/j.epsl.2010.05.022
Miller, I. M., Brandon, M. T., and Hickey, L., 2006, Using leaf margin analysis to estimate the mid-Cretaceous (Albian) paleolatitude of the Baja BC block: Earth and Planetary Science Letters, v. 245, n. 1–2, p. 95–114, http://dx.doi.org/10.1016/j.epsl.2006.02.022
Mitchell, C., Graham, S. A., and Suek, D. H., 2010, Subduction complex uplift and exhumation and its influence on Maastrichtian forearc stratigraphy in the Great Valley Basin, northern San Joaquin Valley, California: Geological Society of America Bulletin, v. 122, n. 11–12, p. 2063–2078, http://dx.doi.org/10.1130/B30180.1
Mitrovica, J. X., Beaumont, C., and Jarvis, G. T., 1989, Tilting of continental interiors by the dynamical effects of subduction: Tectonics, v. 8, n. 5, p. 1079–1094, http://dx.doi.org/10.1029/TC008i005p01079
Mix, H. T., Mulch, A., Kent-Corson, M. L., and Chamberlain, C. P., 2011, Cenozoic migration of topography in the North American Cordillera: Geology, v. 39, n. 1, p. 87–90, http://dx.doi.org/10.1130/G31450.1
Molnar, P., 2010, Deuterium and oxygen isotopes, paleoelevations of the Sierra Nevada, and Cenozoic climate: Geological Society of America Bulletin, v. 122, n. 7–8, p. 1106–1115, http://dx.doi.org/10.1130/B30001.1
Moucha, R., Forte, A. M., Rowley, D. B., Mitrovica, J. X., Simmons, N. A., and Grand, S. P., 2009, Deep mantle forces and the uplift of the Colorado Plateau: Geophysical Research Letters, v. 36, L19310, http://dx.doi.org/10.1029/2009GL039778
Moxon, I. W., and Graham, S. A., 1987, History and controls of subsidence in the Late Cretaceous-Tertiary Great Valley forearc basin, California: Geology, v. 15, n. 7, p. 626–629, http://dx.doi.org/10.1130/0091-7613(1987)15⟨626:HACOSI⟩2.0.CO;2
Mulch, A., and Chamberlain, C. P., 2007, Stable isotope paleoaltimetry in orogenic belts—the silicate record in surface and crustal geological archives: Reviews in Mineralogy and Geochemistry, v. 66, p. 89–118, http://dx.doi.org/10.2138/rmg.2007.66.4
Mulch, A., Graham, S. A., and Chamberlain, C. P., 2006, Hydrogen isotopes in Eocence river gravels and paleoelevation of the Sierra Nevada: Science, v. 313, n. 5783, p. 87–89, http://dx.doi.org/10.1126/science.1125986
Mulch, A., Sarna-Wojcicki, A. M., Perkins, M. E., and Chamberlain, C. P., 2008, A Miocene to Pleistocene climate and elevation record of the Sierra Nevada (California): Proceedings of the National Academy of Sciences of the United States of America, v. 105, n. 19, p. 6819–6824, http://dx.doi.org/10.1073/pnas.0708811105
Oslon, H. C., 1988, Oligocene-middle Miocene depositional systems north of Bakersfield, California; eastern basin equivalents of the Temblor Formation: Field Trip Guidebook—Pacific Section Society of Economic Paleontologists and Mineralogists, v. 60, p. 189–205.
Poage, M. A., and Chamberlain, C. P., 2002, Stable isotopic evidence for a pre-middle Miocene rainshadow in the western Basin and Range: implications for the paleotopography of the Sierra Nevada: Tectonics, v. 21, n. 4, p. 1–10, http://dx.doi.org/10.1029/2001TC001303
Poulsen, C. J., and Jeffery, M. L., 2011, Climate change imprinting on stable isotopic compositions of high-elevation meteoric water cloaks past surface elevations of major orogens: Geology, v. 39, n. 6, p. 595–598, http://dx.doi.org/10.1130/G32052.1
Reiners, P. W., 2007, Thermochronologic approaches to paleotopography, *in* Ehlers, T., and Reiners, P., editors, Low-Temperature Thermochronology: Techniques, Interpretations, Applications: Reviews in Mineralogy and Geochemistry, v. 66, p. 243–267, http://dx.doi.org/10.2138/rmg.2007.66.10
Reiners, P. W., and Brandon, M. T., 2006, Using thermochronology to understand orogenic evolution: Annual Review of Earth and Planetary Sciences, v. 34, p. 419–466, http://dx.doi.org/10.1146/annurev.earth.34.031405.125202
Ruppert, S., Fliedner, M. M., and Zandt, G., 1998, Thin crust and active upper mantle beneath the southern Sierra Nevada in the western United States: Tectonophysics, v. 286, p. 237–252, http://dx.doi.org/10.1016/S0040-1951(97)00268-0
Sambridge, M., 1999a, Geophysical inversion with a neighborhood algorithm—I. Searching a parameter space: Geophysical Journal International, v. 138, n. 2, p. 479–494, http://dx.doi.org/10.1046/j.1365-246X.1999.00876.x
——— 1999b, Geophysical inversion with a neighborhood algorithm—II. Appraising the ensemble: Geophysical Journal International, v. 138, n. 3, p. 727–746, http://dx.doi.org/10.1046/j.1365-246x.1999.00900.x
Schwarz, G., 1978, Estimating the dimension of a model: The Annals of Statistics, v. 6, n. 2, 461–464, http://dx.doi.org/10.1214/aos/1176344136
Shuster, D. L., and Farley, K. A., 2009, The influence of artificial radiation damage and thermal annealing on

helium diffusion kinetics in apatite: Geochimica et Cosmochimica Acta v. 73, n. 1, p. 183–196, http://dx.doi.org/10.1016/j.gca.2008.10.013

Shuster, D. L., Flowers, R. M., and Farley, K. A., 2006, The influence of natural radiation damage on helium diffusion kinetics in apatite: Earth and Planetary Science Letters, v. 249, n. 3–4, p. 148–161, http://dx.doi.org/10.1016/j.epsl.2006.07.028

Sivia, D. S., and Skilling, J., 2006, Data Analysis: a Bayesian tutorial: New York, Oxford University Press, New York, 259 p.

Small, E. E., and Anderson, R. S., 1995, Geomorphically driven Late Cenozoic rock uplift in the Sierra Nevada, California: Science, v. 270, p. 277–281, http://dx.doi.org/10.1126/science.270.5234.277

Stern, T. W., Bateman, P. C., Morgan, B. A., Newell, M. F., and Peck, D. L., 1981, Isotopic U-Pb ages of zircon from the granitoids of the central Sierra Nevada, California: U.S. Geological Survey Professional Paper 1185, 17 p.

Stock, G. M., Anderson, R. S., and Finkel, R. C., 2004, Pace of landscape evolution in the Sierra Nevada, California, revealed by cosmogenic dating of cave sediments: Geology, v. 32, n. 3, p. 193–196, http://dx.doi.org/10.1130/G20197.1

——— 2005, Rates of erosion and topographic evolution of the Sierra Nevada, California, inferred from cosmogenic ^{26}Al and ^{10}Be concentrations: Earth Surface Processes and Landforms, v. 30, p. 985–1006, http://dx.doi.org/10.1002/esp.1258

Tarantola, A., 2005, Inverse problem theory and methods for model parameter estimation: Philadelphia, Pennsylvania, Society for Industrial and Applied Mathematics, 326 p.

Thompson, G. A., and Parsons, T., 2009, Can footwall unloading explain the late Cenozoic uplift of the Sierra Nevada crest?: International Geology Review, v. 51, n. 9–11, p. 986–993, http://dx.doi.org/10.1080/00206810903059156

Unruh, J. R., 1991, The uplift of the Sierra Nevada and implications for late Cenozoic epeirogeny in the western Cordillera: Geological Society of America Bulletin, v. 103, n. 11, p. 1395–1404, http://dx.doi.org/10.1130/0016-7606(1991)103⟨1395:TUOTSN⟩2.3.CO;2

Wackernagel, H., 2003, Multivariate Geostatistics: An Introduction with Applications: New York, Springer, 387 p.

Wagner, G. A., and Reimer, G. M., 1972, Fission track tectonics: the tectonic interpretation of fission track ages: Earth and Planetary Science Letters, v. 14, n. 2, p. 263–268, http://dx.doi.org/10.1016/0012-821X(72)90018-0

Wakabayashi, J., and Sawyer, T. L., 2001, Stream incision, uplift, and evolution of topography of the Sierra Nevada, California: The Journal of Geology, v. 109, p. 539–562, http://dx.doi.org/10.1086/321962

Wernicke, B., Clayton, R., Ducea, M., Jones, C. H., Park, S., Ruppert, S., Saleeby, J., Snow, J. K., Squires, L., Fliedner, M., Jiracek, G., Keller, R., Klemperer, S., Luetgert, J., Malin, P., Miller, K., Mooney, W., Oliver, H., and Phinney, R., 1996, Origin of High Mountains in the Continents: The southern Sierra Nevada: Science, v. 271, n. 5246, p. 190–193, http://dx.doi.org/10.1126/science.271.5246.190

Zandt, G., Gilbert, H., Owens, T. J., Ducea, M., Saleeby, J., and Jones, C. H., 2004, Active foundering of a continental arc root beneath the southern Sierra Nevada in California: Nature, v. 431, p. 41–46, http://dx.doi.org/10.1038/nature02847